

# Dark Matter Minihalos from Primordial Magnetic Fields

Pranjal Ralegankar\*

*SISSA, International School for Advanced Studies, via Bonomea 265, 34136 Trieste, Italy*

Primordial magnetic fields (PMF) can enhance baryon perturbations on scales below the photon mean free path. However, a magnetically driven baryon fluid becomes turbulent near recombination, thereby damping out baryon perturbations below the turbulence scale. In this letter, we show that the growth of baryon perturbations is imprinted in the dark matter perturbations, which are unaffected by turbulence and eventually collapse to form  $10^{-11} - 10^3 M_\odot$  dark matter minihalos. In the process, we analytically derive the evolution of the PMF power spectrum in the viscous drag regime. If the magnetic fields purportedly detected in the blazar observations are PMFs generated after inflation and have a Batchelor spectrum, then such PMFs should also produce minihalos.

**Introduction.** Magnetic fields are found to be ubiquitous in our observations of the universe. An intriguing possibility is that the observed cosmic magnetic fields are seeded by magnetic fields produced in the early universe, either during inflation or phase transition [1, 2]. So far no direct evidence for the primordial nature of the magnetic fields has been obtained. However, the absence of GeV gamma-ray halos around TeV blazars might be a smoking gun signal for primordial magnetic fields [3–7].

If magnetic fields have a primordial origin, then they tend to enhance baryon density perturbations after baryons decouple from photons in the early universe [8–12]. This is because a stochastically distributed magnetic field has a compressible component of the Lorentz force acting on the baryon fluid. When baryons are strongly coupled with the photon bath, the relativistic photon pressure counteracts any growth in baryon density perturbations. But on scales below the photon mean free path, the baryon fluid is decoupled from the photon bath and the compressible Lorentz force can lead to the growth of baryon inhomogeneities.

Earlier works that studied the impact of primordial magnetic fields (PMFs) on the matter power spectrum focussed on length scales larger than the so called magnetic Jeans length and thereby focussed on structures bigger than  $\sim 10^6 M_\odot$  [8, 9, 11, 13–24]. On scales smaller than the magnetic Jeans length, baryon perturbations tend to become non-linear prior to recombination [12, 25, 26]. However, the non-linearities in the baryon fluid eventually lead to turbulence at recombination and all signs of enhanced baryon density perturbations below the magnetic Jeans length are erased by today.

In this letter, we show that even though the small-scale baryon density perturbations are erased, their growth history is imprinted on the dark matter (DM) density distribution. Thus, searches for DM minihalos with masses smaller than  $10^6 M_\odot$  can be used to probe PMFs.

**Magnetic fields in the photon drag regime.** We shall focus on scales smaller than the photon mean free path and on times before recombination. Moreover, we consider scales larger than 0.01 pc, where the baryon fluid can be approximated as a perfect fluid and a perfect con-

ductor prior to recombination. Consequently, the motion of the baryon fluid under the influence of a PMF is given by [10]

$$\frac{\partial \vec{v}_b}{\partial t} + (H + \alpha) \vec{v}_b + \frac{c_b^2}{a} \nabla \delta_b = \frac{\vec{L}_B}{a} - \frac{\nabla \phi}{a}, \quad (1)$$

where  $a$  is the scale factor,  $\vec{v}_b = a d\vec{x}_b/dt$  is the physical baryon velocity,  $\delta = (\rho(x) - \bar{\rho})/\bar{\rho}$  is the fluid density perturbation,  $\phi$  is the metric perturbation following the convention in [27],  $\alpha = 4\rho_\gamma/(3\rho_b l_\gamma)$  parametrizes the photon drag force with  $l_\gamma$  being the photon mean free path,  $\rho_\gamma$  is the photon energy density,  $c_b^2$  is the baryon sound speed and parametrizes the baryon thermal pressure,  $H$  is the Hubble rate, and  $\vec{L}_B = (\nabla \times \vec{B}) \times \vec{B}/[4\pi a^4 \rho_b]$  is the Lorentz force with  $\vec{B} = a^2 \vec{B}_{\text{phys}}$  being the comoving magnetic field and  $\vec{B}_{\text{phys}}$  being the physical magnetic field. The evolution of  $B$  is determined by,

$$\frac{\partial \vec{B}}{\partial t} = \frac{1}{a} \nabla \times (\vec{v}_b \times \vec{B}). \quad (2)$$

We work in natural units where  $\hbar = c = 1$ .

In eq. (1) we have ignored the contribution from convection,  $(\vec{v}_b \cdot \nabla) \vec{v}_b/a$ , because the viscous drag on baryons due to scattering with photons,  $\alpha v_b$ , is much larger than the convective term [28]. One can verify this by using the fact that  $\alpha$  is orders of magnitude larger than  $H$  prior to recombination,  $\alpha/H \sim 350(a_{\text{rec}}/a)^2$ .

In this section, we are interested in computing the evolution of the PMF power spectrum,  $P_B(k, t)$ . For any statistically isotropic and homogeneous PMF, we have

$$\langle B_i(k) B_j^*(k') \rangle = \delta^3(k - k') \frac{P_B(k)}{2} \left( \hat{p}_{ij} + i h(k) \epsilon_{ijl} \frac{k^l}{k} \right), \quad (3)$$

where  $B_i(k) = \int d^3x B_i(x) e^{ikx}$ ,  $\delta^3 = (2\pi)^3 \delta^3$  is the  $2\pi$  normalized Dirac delta function,  $\hat{p}_{ij} = \delta_{ij} - k_i k_j/k^2$ , and  $h(k) P_B(k)$  is the helical power spectrum. With the above convention, PMF energy density is simply  $8\pi \rho_B \equiv \langle B^2 \rangle = \int d\Pi_q P_B(q)$ , where  $d\Pi_q = d^3q/(2\pi)^3$ .

Taking the time derivative of eq. (3) and replacing  $\partial B/\partial t$  using eq. (2) would yield the evolution equations for  $P_B$  and  $h$ . We can make further analytical progress by

noting that in eq. (1),  $(\alpha + H)v_b \gg \partial v_b / \partial t \sim H v_b$  before recombination. Then if the Lorentz force dominates over thermal pressure and gravity, we have  $a\vec{v}_b \approx \vec{L}_B / (\alpha + H)$ . Working in this large Lorentz force limit and neglecting non-Gaussianities in the distribution of  $B$ , we obtain

$$\frac{\partial P_B(k)}{\partial t} = \frac{-P_B(k)/3}{\pi\rho_b(\alpha + H)} \int d\Pi_q k [k - qh(k)h(q)] P_B(q), \quad (4)$$

$$\frac{\partial h(k)}{\partial t} = \frac{k/3}{\pi\rho_b(\alpha + H)} [1 - h^2(k)] \int d\Pi_q q h(q) P_B(q). \quad (5)$$

From above we can see that if initially  $h \neq 0$ , then the PMF is eventually driven to the maximally helical configuration,  $|h| \rightarrow 1$ , as expected [29]. One can also confirm that the PMF helical density,  $\int d\Pi_q h(q) P_B(q)/q$ , is conserved under the above equations and that the equations reproduce the inverse cascade of power for maximally helical fields ( $h = 1$ ) (See appendices at the end [30]). To our knowledge, we are the first to provide an analytical evolution equation for  $P_B$  with arbitrary helicity in the photon drag regime.

In the remainder of the paper, we shall focus on non-helical PMFs,  $h(k) = 0$ , for simplicity. In this limit, the solution to eq. (4) is given by

$$P_B(k, k_D(t)) = P_B(k, t_i) e^{-k^2/k_D^2}, \quad (6)$$

where  $k_D$  represents the damping scale due to photon drag, and  $P_B(k, t_i)$  is the power spectra prior to the photon drag regime, i.e. when the PMF coherence length scale was larger than the photon diffusion length,  $l_{\gamma D} \approx 1/4\sqrt{l_\gamma/[aH]}$ . Substituting the above solution back in eq. (4), we obtain

$$a \frac{\partial}{\partial a} \left( \frac{1}{k_D^2} \right) = \frac{4V_A^2/3}{a^2 H(\alpha + H)}, \quad (7)$$

where  $V_A^2 = \langle B^2 \rangle / (4\pi a^4 \rho_b)$  is the Alfvén speed. Given that  $a\vec{v}_b \approx \vec{L}_B / (\alpha + H)$  and  $L_B \sim k_D V_A^2$ , eq. (7) tells us that the damping scale is roughly the distance a baryon particle travels in a Hubble time,  $ak_D^{-1} \sim v_b/H \sim k_D V_A^2 / [aH(\alpha + H)]$ . The above equation agrees with the free-streaming Alfvén damping scale derived for pre-recombination universe ( $\alpha \gg H$ ) by Ref. [31], as well as with the magnetic Jeans damping scale derived for post-recombination universe ( $\alpha \ll H$ ) by Ref. [9, 10].

We have neglected the effect of thermal pressure and gravity while deriving eq. (7). We find that even if thermal pressure dominates over the Lorentz force, the damping scale is roughly determined by the same scale as in eq. (7) (See appendices at the end [30]; see also [31]). Furthermore, for PMFs that produce observable enhancement in the DM power spectrum, we find gravity to be subdominant to the Lorentz force for  $k \lesssim k_D$ . Consequently, we approximate the damping scale to be given by eq. (7) in all regimes.

In the top panel of figure 1, the green line shows the evolution of the damping scale,  $k_D^{-1}$ . Here and in the remaining letter, we consider PMFs with a Batchelor spectrum, i.e.  $P_B(k, t_i) \propto k^2$  for  $k < \xi_I^{-1}$  and  $P_B \propto k^{-11/3}$  for  $k > \xi_I^{-1}$ . We borrow the exact shape of  $P_B(k, t_i)$  from Ref. [32]. We have rescaled  $P_B(k, t_i)$  to obtain desired initial PMF strength,  $B_I \equiv \langle B^2(t_i) \rangle$ , and initial coherence length scale,  $\xi_I \equiv B_I^{-2} \int d\Pi_q P_B(q, t_i)/q$ . We have solved the background cosmology parameters ( $H$ ,  $\alpha$ ,  $\rho$ , etc.) using CLASS [33].

In figure 1, one can see that  $k_D^{-1}$  grows as  $a^{3/2}$  when  $k_D^{-1} \lesssim \xi_I$  and as  $k_D^{-1} \propto a^{3/7}$  after  $k_D^{-1} > \xi_I$ . This transition occurs because when  $k_D^{-1} < \xi_I$  the PMF is flux frozen (constant  $\langle B^2 \rangle$ ) but afterwards the PMF is damped as  $\langle B^2 \rangle \propto k_D^5 \propto a^{-15/14}$ . The sudden increase in  $k_D^{-1}$  near recombination is due to the rapid decrease in photon drag,  $\alpha$ .

After recombination, the MHD fluid becomes turbulent and this turbulence is not captured in our formalism. Nevertheless, we extend eq. (7) beyond recombination and find a logarithmic growth of  $k_D^{-1}$ , which is also expected from simulations [28]. Consequently, our evaluation of present-day values of  $B$  and  $k_D$  should be accurate up to an order of magnitude.

**Impact on baryon density perturbations.** The continuity equation for  $\delta_b$  in the linear limit is

$$\frac{\partial \delta_b}{\partial t} + \frac{\nabla \cdot \vec{v}_b}{a} = 0. \quad (8)$$

We find that the non-linear term in the continuity equation,  $\nabla \cdot (\delta_b \vec{v}_b)/a$ , tends to enhance the power spectrum of  $\delta_b$  by  $\sim 10\%$  when baryons are driven by the Lorentz force (See appendices at the end [30]). We found this by taking the ensemble average of the continuity equation convolved with  $\delta_b(x')$  and using the linear solution,  $\delta_b \propto \nabla \cdot v_b / [aH] = a^{-2} \nabla \cdot L_B / [H(\alpha + H)]$ . As we are not interested in a precision calculation of the DM power spectrum, we have ignored the non-linear term here.

In the bottom panel of figure 1, we show the evolution of  $\hat{\delta}_b \equiv \sqrt{k^3 P_b(k)/(2\pi^2)}$  for two different Fourier modes, where  $P_b$  is the baryon power spectrum. We start our computation when the photon mean free path exceeds the initial coherence length scale,  $l_\gamma(t'_i) > \xi_I$ . We set  $\delta_b(t'_i) = v_b(t'_i) = 0$ , which is expected due to silk damping. Here  $v_b$  is solved using eq. (1).

The evolution of  $\delta_b$  can roughly be classified into four regimes. In the first regime,  $\delta_b$  grows as  $\sim a^3$  due to the Lorentz force. The growth eventually stops when the damping scale exceeds the length scale of the Fourier mode,  $k_D^{-1} \gtrsim 3k^{-1}$ , because the Lorentz force is damped out.

Our evaluation of  $\hat{\delta}_b$  for  $k_D^{-1} \gtrsim k$  is not completely accurate. This is because we have approximated the evolution of  $\nabla \cdot \vec{L}_B(k, t)$  to be the same as  $\sqrt{\langle (\nabla \cdot \vec{L}_B(k, t))^2 \rangle}$ , which is not true due to non-linear processing between

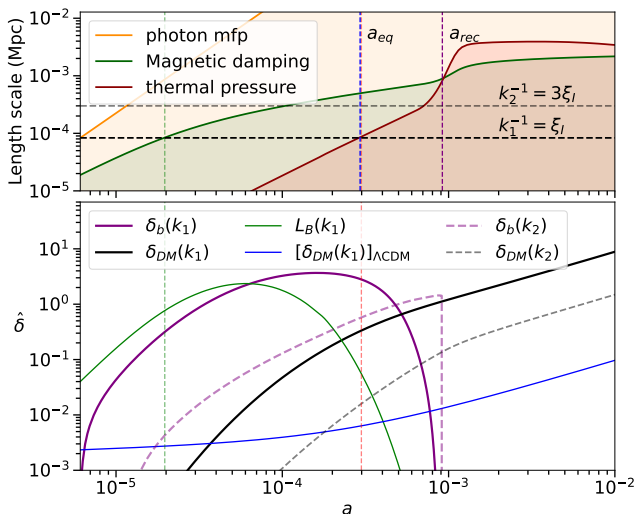


FIG. 1. This figure takes  $B_I = 5$  nG and  $\xi_I = 10^{-4}$  Mpc. **Top:** Evolution of the photon mean free path (orange), the magnetic damping scale  $k_D^{-1}$  (green), and the thermal pressure damping scale  $\lambda_{th}$  (red). Horizontal dashed lines mark the comoving wavenumbers corresponding to perturbations shown in the bottom panel. **Bottom:** Evolution of the square root of dimensionless power spectra,  $\hat{\delta} = \sqrt{k^3 P/(2\pi^2)}$ . The green line shows  $\hat{\delta}$  for  $a^{-2}\nabla \cdot \vec{L}_B/[H(\alpha + H)]$ . The blue line shows  $\hat{\delta}_{DM}$  in a universe with no PMF, while other lines correspond to perturbations sourced by PMFs assuming trivial initial condition. Vertical green and red dashed lines mark the time when  $k_1^{-1}$  crosses  $k_D^{-1}$  and  $\lambda_{th}$ , respectively.

different Fourier modes of PMF. However, for the purpose of calculating  $P_b(k, t)$ , this approximation is acceptable because when baryons are driven by  $L_B$ , we have  $\delta_b \propto a^{-2}\nabla \cdot \vec{L}_B/(\alpha + H)$ . Consequently,  $P_b$  is directly determined by  $\langle (\nabla \cdot \vec{L}_B(k, t))^2 \rangle$ . Furthermore, once  $\vec{L}_B$  is damped for  $k \gg k_D$ ,  $\delta_b$  is no longer sensitive to our approximation in  $\vec{L}_B(k)$ . In the transition regime, we expect no more than  $\mathcal{O}(1)$  correction to  $P_b$ .

The second regime of  $\delta_b$  evolution corresponds to saturation, where  $v_b$  is quickly driven to zero by the photon drag and  $\delta_b$  saturates to a constant. If baryon thermal pressure is ignored,  $\delta_b$  asymptotes to  $\sim \mathcal{O}(1)$  values for  $k \gg k_D$ . This  $\mathcal{O}(1)$  asymptote is just a reflection of the fact that  $k_D$  is determined by the distance traveled by a baryon particle in a Hubble time,  $k_D^{-1} \sim v_b/(aH)$ , which translates to  $\delta_b \sim \mathcal{O}(1)$  as  $\delta_b \sim kv_b/(aH)$ .

The third regime corresponds to the damping of  $\delta_b$  by thermal pressure. The thermal pressure becomes important when the thermal force becomes of the same order as the photon drag force,  $c_b^2 k \delta_b \sim (H + \alpha)v_b$ . Using  $\delta_b \sim kv_b/(aH)$ , we find the thermal pressure damping scale to be

$$\lambda_{th} = \frac{c_b}{aH} \sqrt{\frac{H}{\alpha + H}}. \quad (9)$$

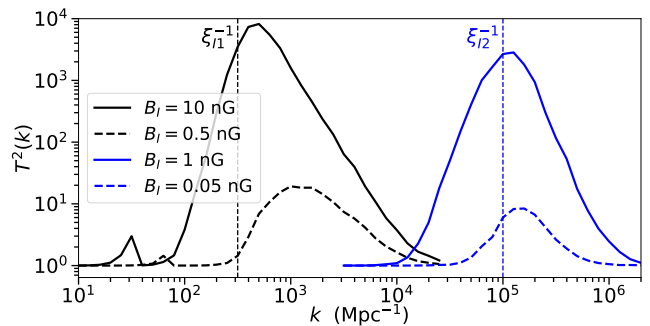


FIG. 2. The dark matter transfer function for PMF configurations sampling the edges of the parameter space shown in figure 3.

We plot this scale as a red line in the top panel of figure 1.

Finally, the fourth regime corresponds to turbulence damping near recombination. At recombination, the photon drag force almost instantaneously becomes negligible and the convective terms in the baryon Euler equation (eq. (1)) can no longer be ignored [25, 26, 28]. We model the impact of turbulence on  $\delta_b$  by setting  $\delta_b = 0$  at recombination for all scales inside the magnetic damping scale.

**Impact on DM perturbations.** The rapid growth in  $\delta_b$  gravitationally induces growth in DM perturbations,  $\delta_{DM}$ . However, we find that  $\delta_{DM}$  largely remains in the perturbative regime before recombination even if  $\delta_b$  reaches non-linear values. This is because the gravitational influence of baryons is suppressed by a factor of  $\rho_b/\rho_{tot}$ . Consequently, the growth in  $\delta_{DM}$  is well captured by the linear theory [27],

$$a^2 \frac{\partial^2 \delta_{DM}}{\partial a^2} + a \left[ \frac{\partial \ln(a^2 H)}{\partial \ln a} + 1 \right] \frac{\partial \delta_{DM}}{\partial a} - \frac{3}{2} \frac{\Omega_{DM}}{\Omega_m} \frac{\delta_{DM}}{1 + a_{eq}/a} = \frac{3}{2} \frac{\Omega_b}{\Omega_m} \frac{\delta_b}{1 + a_{eq}/a}. \quad (10)$$

Here  $\Omega$  corresponds to the present day fraction of species, with  $\Omega_b h^2 = 0.022$ ,  $\Omega_{DM} h^2 = 0.12$ ,  $\Omega_m = \Omega_b + \Omega_{DM}$ , and  $a_{eq}$  is the scale factor at matter radiation equality [34]. The contribution of radiation perturbations have been neglected above because they are damped by free-streaming.

Since  $\delta_{DM}$  follows an ordinary differential equation, its solution can simply be written as a linear combination of the homogenous solution provided by the initial condition and the inhomogeneous solution indirectly sourced by PMF,  $\delta_{DM} = (\delta_{DM})_{\Lambda CDM} + (\delta_{DM})_B$ . As the PMF distribution is uncorrelated with the curvature perturbations determining initial conditions [34], the two solutions of  $\delta_{DM}$  are uncorrelated as well.

In figure 2, we show the DM transfer function,  $T^2(k) = P_{DM}(k)/[P_{DM}(k)]_{\Lambda CDM}$ , where  $P_{DM}$  is the DM power spectrum,  $\bar{\delta}^3(k - k') P_{DM}(k) = \langle \delta_{DM}(k) \delta_{DM}(k') \rangle_B +$

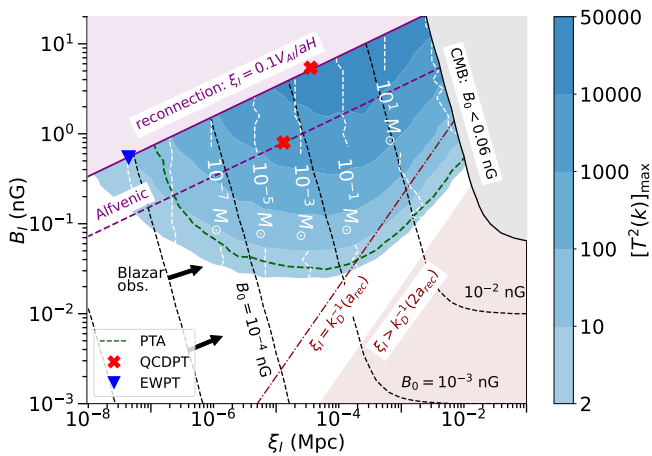


FIG. 3. Colored contours of the maximum value of dark matter transfer function as a function of initial comoving magnetic field strength,  $B_I$ , and initial coherence length scale,  $\xi_I$ . Here initial refers to the time when the photon diffusion length becomes larger than  $\xi_I$ . White contours show the mass scales at which the transfer function reaches its peak. Black dashed lines show the contours of present-day magnetic field strength,  $B_0$ . The region inside the green-dashed line produce dark matter minihalos potentially within the observable reach of PTAs. Solid and dashed purple lines denote the relation between  $\xi_I$  and  $B_I$  depending on whether MHD turbulence is determined by reconnection or Alfvénic physics, respectively. The red crosses (blue triangle) mark the maximum values of  $B_I$  for PMFs produced during QCD (electroweak) phase transition.

$\langle \delta_{DM}(k)\delta_{DM}(k') \rangle_{\Lambda CDM}$ . One can see that the transfer function is quite narrowly peaked with the peak typically occurring at  $k_{pk} \sim \xi_I^{-1}$ . For  $k < k_{pk}$ , thermal pressure or turbulence at recombination suppresses  $\delta_b$  before it attains its maximum value due to the Lorentz force. The value of  $k_{pk}$  for the black dashed line is shifted to  $k_{pk} > \xi_I^{-1}$ , because  $\delta_b(k = \xi_I^{-1})$  is prematurely suppressed by turbulence at recombination. The value of  $T(k)$  for  $k > \xi_I$  is suppressed because the initial magnetic fields are itself suppressed on such small scales.

**Connecting PMFs with DM minihalos.** In figure 3 we vary over different initial PMF configurations and plot the contours showing the maximum enhancement to the DM transfer function,  $[T^2(k)]_{\max}$ . A larger value of  $[T^2(k)]_{\max}$  imply that the halos corresponding to the peak scale,  $k_{pk}^{-1}$ , collapse earlier than in standard cosmology and consequently have much larger central densities [35–37]. The mass of these first formed minihalos is approximately given by the DM mass enclosed in a radius of  $ak_{pk}^{-1}$ , i.e.  $M_h = 4\pi\rho_{DM}(a=1)k_{pk}^{-3}/3$ .

The value of  $[T^2(k)]_{\max}$  is suppressed for small  $B_I$  and for both large and small  $\xi_I$ . When  $B_I < 0.05$  nG, the thermal pressure inhibits the growth in  $\delta_b(k_{pk})$  before it attains its  $\mathcal{O}(1)$  saturation value, which then limits the growth in  $\delta_{DM}$ . For  $\xi_I < 10^{-4}$  Mpc,  $\delta_b(k_{pk})$  is suppressed

by thermal pressure before  $a_{eq}$ . Consequently, the gravitational influence of baryons on DM is suppressed by a factor of  $\sim a/a_{eq}$ . Finally, for  $\xi_I \gtrsim k_D^{-1}(a_{rec})$ , turbulence near recombination suppresses  $\delta_b$  before it can attain  $\mathcal{O}(1)$  values.

For  $\xi_I$  larger than  $k_D^{-1}(2a_{rec})$ , which is roughly the magnetic Jeans length, turbulence at recombination does not affect perturbations on scale  $\xi_I$ . Thus, one can also obtain an enhancement in  $T(k)$  for  $\xi_I > k_D^{-1}(2a_{rec})$  [9, 11, 17]. In this letter, we have restricted our analysis to  $\xi_I < k_D^{-1}(2a_{rec})$ .

Additionally,  $\xi_I$  has a natural lower bound for a given value of  $B_I$ . In particular, prior to the photon drag regime, PMFs induce turbulent motion in the plasma and are damped by Kolmogorov cascade below the turbulence scale,  $\xi_T$ . Consequently,  $\xi_I \geq \xi_T$ . If Alfvénic physics determines MHD turbulence, then  $\xi_T \sim V_{AI}/[aH]_i$ , where  $V_{AI} = B_I/\sqrt{4\pi a^4(4\rho_\gamma/3)}$  [28, 38]. Although, recently it has been argued that a reconnection-controlled MHD turbulence leads to a better agreement with simulations [39, 40]. In this case  $\xi_T \sim 0.1V_{AI}/[aH]_i$  for  $B_I$  values of our interest [41]. In both cases,  $V_{AI}$  and  $aH$  are computed at time  $t_i$  when  $\xi_T$  becomes smaller than the photon diffusion length and the Reynolds number of the plasma falls below unity [28].

If PMFs are generated after inflation, then  $\xi_I = \xi_T$ . Or equivalently,  $B_I$  and  $\xi_I$  lie on one of the purple lines in figure 3, depending on the physics controlling MHD turbulence. The red crosses on the purple lines mark the largest values of  $B_I$  from magnetogenesis at QCD phase transition. This value is calculated assuming  $\rho_B = \rho_{SM}$  and  $\xi_I = (aH)^{-1}$  at  $T_{QCD} = 150$  MeV, and considering  $B^4\xi^5$  to be conserved in the subsequent reconnection-controlled turbulent evolution [39], or considering  $B^2\xi^5$  to be conserved for Alfvénic turbulence. Similarly, the blue triangle corresponds to magnetogenesis at electroweak phase transition at  $T_{EWPT} = 160$  GeV.

PMFs generated after inflation can explain the absence of GeV gamma-ray halos around TeV blazars, if their present day strength,  $B_0 = \langle B^2(a=1) \rangle$ , is larger than  $\sim 10^{-5}$  nG [42]. One can see that PMFs generated after EWPT can explain Blazar observations [41] and also enhance the small-scale matter power spectrum.

An enhancement in  $[T^2(k)]_{\max}$  implies an enhanced abundance of minihalos today. The presence of such minihalos in the Milkyway can potentially be observed by astrometric microlensing searches [43–45], caustic microlensing [46, 47], or by pulsar timing arrays (PTAs) [48–51]. For instance, the region inside the green-dashed line has  $P_{DM}(k)$  which is potentially in the observable window of future PTA measurements [51]. Note that this is a heuristic estimate and a more detailed analysis is required to draw any definitive conclusion on observability.

Magnetic fields generated during inflation can have

any  $B_I$  and  $\xi_I$  values below the purple lines, as long as they are in agreement with constraints from present day observations. The current strongest constraint restricts  $B_0 < 0.06$  nG [52].

A further stringent constraint of  $B_0 < 0.01$  nG can be applied if  $\xi_I$  is close to  $k_D^{-1}(a_{\text{rec}})$ . For these  $\xi_I$  values,  $\delta_b$  becomes non-linear near recombination and hence affects recombination history [25]. Recently, this fact has instead been utilized to help resolve the Hubble tension [53]. Depending on the exact values of  $B_I$  and  $\xi_I$  that resolve the Hubble tension, it is possible that an observable abundance of DM minihalos is also produced.

**Discussion.** Magnetic fields can naturally have a primordial origin. We have shown for the first time that such primordial magnetic fields (PMFs) can indirectly enhance the present-day matter power spectrum on scales below the magnetic Jeans length. While we showed the above for non-helical PMFs with a Batchelor spectrum, other PMF configurations should also produce significant enhancement to the small-scale matter power spectrum.

Using analytical calculations in the photon drag regime, and considering non-helical PMFs generated after inflation with a Batchelor spectrum, we estimate that PMFs that can explain blazar observations should also produce dark matter minihalos heavier than  $10^{-10} M_\odot$ . Such minihalos can potentially be probed by future PTA measurements. Although dedicated MHD and structure formation simulations are required to obtain an accurate spectrum of minihalos and gauge their observability.

To our knowledge, we are the first to provide an analytical evolution of the PMF power spectrum in the photon drag regime. The only major assumption in our analysis is that we neglected non-gaussianities in the PMF distribution. The fact that our analytical formalism can reproduce the expected behavior of magnetic fields, including inverse energy cascade for maximally helical fields [30], seems to suggest that non-gaussianities do not play a major role in the photon drag regime. However, if non-gaussianities somehow alter the PMF evolution through reconnection physics, we expect that would only further enhance the density perturbations. This is because reconnection typically leads to a slower damping of PMFs than expected, thereby allowing more time for perturbations to grow.

In conclusion, a future detection of dark matter minihalos should serve as a smoking gun signal for a primordial origin of cosmic magnetic fields. It is rather ironic how we can utilize the invisible component of our universe to search for a component of the visible sector.

*Acknowledgments.* The author thanks Karsten Jedamzik for clarification about initial magnetic field configurations and cross-checking some calculations, Kandaswamy Subramanian for initial guidance on relevant literature, Takeshi Kobayashi for several helpful discussions, Adrienne Erickcek for clarification on minihalos and help-

ful discussions, Andrea Mitridate for clarification about PTA sensitivities, and Andrey Saveliev for clarifications about his work and highlighting different conventions used for PMF power spectra. The author is also thankful to Karsten Jedamzik, Takeshi Kobayashi, and Jan Schutte-Engel for helpful feedback on the manuscript.

---

\* pralegan@sissa.it

- [1] T. Vachaspati, Progress on cosmological magnetic fields, Rept. Prog. Phys. **84**, 074901 (2021), arXiv:2010.10525 [astro-ph.CO].
- [2] K. Subramanian, The origin, evolution and signatures of primordial magnetic fields, Rept. Prog. Phys. **79**, 076901 (2016), arXiv:1504.02311 [astro-ph.CO].
- [3] A. Neronov and I. Vovk, Evidence for strong extragalactic magnetic fields from fermi observations of tev blazars, Science **328**, 73 (2010), <https://www.science.org/doi/pdf/10.1126/science.1184192>.
- [4] A. Abramowski *et al.* (H.E.S.S.), Search for Extended  $\gamma$ -ray Emission around AGN with H.E.S.S. and Fermi-LAT, Astron. Astrophys. **562**, A145 (2014), arXiv:1401.2915 [astro-ph.HE].
- [5] J. D. Finke, L. C. Reyes, M. Georganopoulos, K. Reynolds, M. Ajello, S. J. Fegan, and K. McCann, Constraints on the Intergalactic Magnetic Field with Gamma-Ray Observations of Blazars, Astrophys. J. **814**, 20 (2015), arXiv:1510.02485 [astro-ph.HE].
- [6] S. Archambault *et al.* (VERITAS), Search for Magnetically Broadened Cascade Emission From Blazars with VERITAS, Astrophys. J. **835**, 288 (2017), arXiv:1701.00372 [astro-ph.HE].
- [7] R. Alves Batista and A. Saveliev, The Gamma-ray Window to Intergalactic Magnetism, Universe **7**, 223 (2021), arXiv:2105.12020 [astro-ph.HE].
- [8] I. Wasserman, On the origins of galaxies, galactic angular momenta, and galactic magnetic fields., Astrophys. J. **224**, 337 (1978).
- [9] E.-j. Kim, A. Olinto, and R. Rosner, Generation of density perturbations by primordial magnetic fields, Astrophys. J. **468**, 28 (1996), arXiv:astro-ph/9412070.
- [10] K. Subramanian and J. D. Barrow, Magnetohydrodynamics in the early universe and the damping of non-linear Alfvén waves, Phys. Rev. D **58**, 083502 (1998), arXiv:astro-ph/9712083.
- [11] R. Gopal and S. K. Sethi, Large Scale Magnetic Fields: Density Power Spectrum in Redshift Space, Journal of Astrophysics and Astronomy **24**, 51 (2003).
- [12] K. Jedamzik and T. Abel, Small-scale primordial magnetic fields and anisotropies in the cosmic microwave background radiation, **2013**, 050 (2013).
- [13] S. K. Sethi and K. Subramanian, Primordial magnetic fields in the post-recombination era and early reionization, Mon. Not. Roy. Astron. Soc. **356**, 778 (2005), arXiv:astro-ph/0405413.
- [14] H. Tashiro and N. Sugiyama, Early reionization with primordial magnetic fields, Mon. Not. Roy. Astron. Soc. **368**, 965 (2006), arXiv:astro-ph/0512626 [astro-ph].
- [15] D. R. G. Schleicher, R. Banerjee, and R. S. Klessen, Influence of primordial magnetic fields on 21 cm emission, Astrophys. J. **692**, 236 (2009), arXiv:0808.1461 [astro-

- ph].
- [16] S. K. Sethi and K. Subramanian, Primordial magnetic fields and the HI signal from the epoch of reionization, *JCAP* **2009** (11), 021, arXiv:0911.0244 [astro-ph.CO].
- [17] J. R. Shaw and A. Lewis, Constraining Primordial Magnetism, *Phys. Rev. D* **86**, 043510 (2012), arXiv:1006.4242 [astro-ph.CO].
- [18] K. L. Pandey and S. K. Sethi, Theoretical Estimates of Two-point Shear Correlation Functions using Tangled Magnetic Fields, *Astrophys. J.* **748**, 27 (2012), arXiv:1201.3619 [astro-ph.CO].
- [19] K. L. Pandey and S. K. Sethi, Probing Primordial Magnetic Fields Using Ly $\alpha$  Clouds, *Astrophys. J.* **762**, 15 (2013), arXiv:1210.3298 [astro-ph.CO].
- [20] S. Chongchitnan and A. Meiksin, The effect of cosmic magnetic fields on the metagalactic ionization background inferred from the Lyman  $\alpha$  forest, *Mon. Not. Roy. Astron. Soc.* **437**, 3639 (2014), arXiv:1311.1504 [astro-ph.CO].
- [21] K. L. Pandey, T. R. Choudhury, S. K. Sethi, and A. Ferrara, Reionization constraints on primordial magnetic fields, *Mon. Not. Roy. Astron. Soc.* **451**, 1692 (2015), arXiv:1410.0368 [astro-ph.CO].
- [22] T. Minoda, K. Hasegawa, H. Tashiro, K. Ichiki, and N. Sugiyama, Thermal Sunyaev-Zel'dovich effect in the intergalactic medium with primordial magnetic fields, *Phys. Rev. D* **96**, 123525 (2017), arXiv:1705.10054 [astro-ph.CO].
- [23] M. Sanati, Y. Revaz, J. Schober, K. E. Kunze, and P. Jablonka, Constraining the primordial magnetic field with dwarf galaxy simulations, *Astronomy and Astrophysics* **643**, A54 (2020).
- [24] H. Katz, S. Martin-Alvarez, J. Rosdahl, T. Kimm, J. Blaizot, M. G. Haehnelt, L. Michel-Dansac, T. Garel, J. Oñorbe, J. Devriendt, A. Slyz, O. Attia, and R. Teyssier, Introducing SPHINX-MHD: the impact of primordial magnetic fields on the first galaxies, reionization, and the global 21-cm signal, *Mon. Not. Roy. Astron. Soc.* **507**, 1254 (2021), arXiv:2101.11624 [astro-ph.CO].
- [25] K. Jedamzik and A. Saveliev, Stringent Limit on Primordial Magnetic Fields from the Cosmic Microwave Background Radiation, *Phys. Rev. Lett.* **123**, 021301 (2019), arXiv:1804.06115 [astro-ph.CO].
- [26] P. Trivedi, J. Reppin, J. Chluba, and R. Banerjee, Magnetic heating across the cosmological recombination era: Results from 3D MHD simulations, *Mon. Not. Roy. Astron. Soc.* **481**, 3401 (2018), arXiv:1805.05315 [astro-ph.CO].
- [27] C.-P. Ma and E. Bertschinger, Cosmological perturbation theory in the synchronous and conformal Newtonian gauges, *Astrophys. J.* **455**, 7 (1995), arXiv:astro-ph/9506072.
- [28] R. Banerjee and K. Jedamzik, The Evolution of cosmic magnetic fields: From the very early universe, to recombination, to the present, *Phys. Rev. D* **70**, 123003 (2004), arXiv:astro-ph/0410032.
- [29] H. K. Moffatt, *Magnetic field generation in electrically conducting fluids* (1978).
- [30] See supplemental material for the analytically derived evolution of maximally helical magnetic fields, for the derivation of damping scale when thermal pressure is dominant, and for the estimate of the non-linear term in the baryon continuity equation., .
- [31] K. Jedamzik, V. Katalinic, and A. V. Olinto, Damping of cosmic magnetic fields, *Phys. Rev. D* **57**, 3264 (1998), arXiv:astro-ph/9606080.
- [32] S. Mtschedlize, P. Domínguez-Fernández, X. Du, A. Brandenburg, T. Kahniashvili, S. O'Sullivan, W. Schmidt, and M. Brüggen, Evolution of Primordial Magnetic Fields during Large-scale Structure Formation, *Astrophys. J.* **929**, 127 (2022), arXiv:2109.13520 [astro-ph.CO].
- [33] D. Blas, J. Lesgourgues, and T. Tram, The Cosmic Linear Anisotropy Solving System (CLASS). Part II: Approximation schemes, *JCAP* **2011** (7), 034, arXiv:1104.2933 [astro-ph.CO].
- [34] N. Aghanim *et al.* (Planck), Planck 2018 results. VI. Cosmological parameters, (2018), arXiv:1807.06209 [astro-ph.CO].
- [35] J. S. Bullock, T. S. Kolatt, Y. Sigad, R. S. Somerville, A. V. Kravtsov, A. A. Klypin, J. R. Primack, and A. Dekel, Profiles of dark haloes. Evolution, scatter, and environment, *Mon. Not. Roy. Astron. Soc.* **321**, 559 (2001), arXiv:astro-ph/9908159.
- [36] R. H. Wechsler, J. S. Bullock, J. R. Primack, A. V. Kravtsov, and A. Dekel, Concentrations of dark halos from their assembly histories, *Astrophys. J.* **568**, 52 (2002), arXiv:astro-ph/0108151.
- [37] M. S. Delos, M. Bruff, and A. L. Erickcek, Predicting the density profiles of the first halos, *Phys. Rev. D* **100**, 023523 (2019), arXiv:1905.05766 [astro-ph.CO].
- [38] T. Kahniashvili, A. G. Tevzadze, A. Brandenburg, and A. Neronov, Evolution of Primordial Magnetic Fields from Phase Transitions, *Phys. Rev. D* **87**, 083007 (2013), arXiv:1212.0596 [astro-ph.CO].
- [39] D. N. Hosking and A. A. Schekochihin, Reconnection-controlled decay of magnetohydrodynamic turbulence and the role of invariants, *Phys. Rev. X* **11**, 041005 (2021).
- [40] H. Zhou, R. Sharma, and A. Brandenburg, Scaling of the Hosking integral in decaying magnetically dominated turbulence, *J. Plasma Phys.* **88**, 905880602 (2022), arXiv:2206.07513 [physics.plasm-ph].
- [41] D. N. Hosking and A. A. Schekochihin, Cosmic-void observations reconciled with primordial magnetogenesis, (2022), arXiv:2203.03573 [astro-ph.CO].
- [42] A. M. Taylor, I. Vovk, and A. Neronov, Extragalactic magnetic fields constraints from simultaneous GeV-TeV observations of blazars, *Astron. Astrophys.* **529**, A144 (2011), arXiv:1101.0932 [astro-ph.HE].
- [43] A. L. Erickcek and N. M. Law, Astrometric Microlensing by Local Dark Matter Subhalos, *Astrophys. J.* **729**, 49 (2011), arXiv:1007.4228 [astro-ph.CO].
- [44] F. Li, A. L. Erickcek, and N. M. Law, A new probe of the small-scale primordial power spectrum: astrometric microlensing by ultracompact minihalos, *Phys. Rev. D* **86**, 043519 (2012), arXiv:1202.1284 [astro-ph.CO].
- [45] K. Van Tilburg, A.-M. Taki, and N. Weiner, Halometry from Astrometry, *JCAP* **07**, 041, arXiv:1804.01991 [astro-ph.CO].
- [46] M. Oguri, J. M. Diego, N. Kaiser, P. L. Kelly, and T. Broadhurst, Understanding caustic crossings in giant arcs: characteristic scales, event rates, and constraints on compact dark matter, *Phys. Rev. D* **97**, 023518 (2018), arXiv:1710.00148 [astro-ph.CO].
- [47] J. M. Diego *et al.*, Dark Matter under the Microscope: Constraining Compact Dark Matter with Caustic Crossing Events, *Astrophys. J.* **857**, 25 (2018),



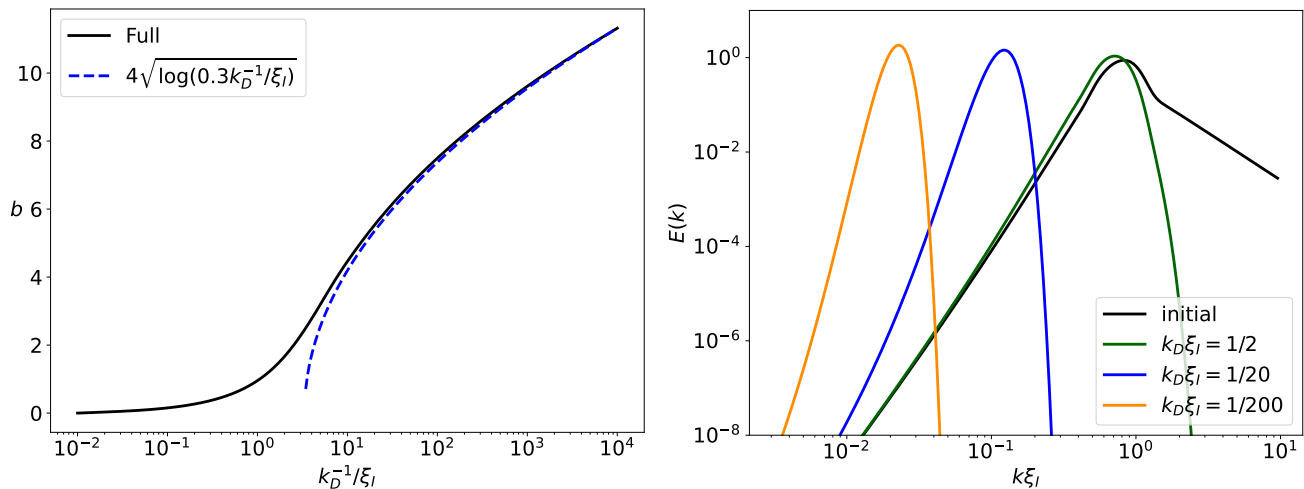


FIG. 4. **left:** Inverse cascade parameter  $b$  as a function of the damping scale  $k_D^{-1}$ . **Right:** Arbitrarily normalized  $E(k) = k^2 P_B(k)$  for different  $k_D$  values. The initial power spectrum is taken to be of that of causally generated helical magnetic fields in freely decaying MHD turbulence [32].

arXiv:1706.10281 [astro-ph.CO].

- [48] E. R. Siegel, M. P. Hertzberg, and J. N. Fry, Probing Dark Matter Substructure with Pulsar Timing, *Mon. Not. Roy. Astron. Soc.* **382**, 879 (2007), arXiv:astro-ph/0702546.
- [49] H. A. Clark, G. F. Lewis, and P. Scott, Investigating dark matter substructure with pulsar timing – I. Constraints on ultracompact minihaloes, *Mon. Not. Roy. Astron. Soc.* **456**, 1394 (2016), [Erratum: *Mon. Not. Roy. Astron. Soc.* 464, 2468 (2017)], arXiv:1509.02938 [astro-ph.CO].
- [50] H. Ramani, T. Trickle, and K. M. Zurek, Observability of Dark Matter Substructure with Pulsar Timing Correlations, *JCAP* **12**, 033, arXiv:2005.03030 [astro-ph.CO].
- [51] V. S. H. Lee, A. Mitridate, T. Trickle, and K. M. Zurek, Probing Small-Scale Power Spectra with Pulsar Timing Arrays, *JHEP* **06**, 028, arXiv:2012.09857 [astro-ph.CO].
- [52] D. Paoletti, J. Chluba, F. Finelli, and J. A. Rubiño Martín, Constraints on Primordial Magnetic Fields from their impact on the ionization history with Planck 2018 10.1093/mnras/stac2947 (2022), arXiv:2204.06302 [astro-ph.CO].
- [53] K. Jedamzik and L. Pogosian, Relieving the Hubble tension with primordial magnetic fields, *Phys. Rev. Lett.* **125**, 181302 (2020), arXiv:2004.09487 [astro-ph.CO].
- [54] P. A. R. Ade *et al.* (Planck), Planck 2015 results. XIX. Constraints on primordial magnetic fields, *Astron. Astrophys.* **594**, A19 (2016), arXiv:1502.01594 [astro-ph.CO].

### Evolution of helical Magnetic field power spectrum

In this section we discuss the evolution of maximally helical magnetic field power spectrum in the viscous damping regime. Prior to this regime, the magnetic fields induce turbulent motion in the baryon-photon plasma and hence the evolution is determined by freely decaying MHD turbulence. The turbulent motion primarily occurs on length scales smaller than the coherence length scale of the magnetic fields. However, once the coherence length scale becomes smaller than the silk damping scale, all motion in the baryon fluid is damped out by the photon diffusion. Consequently, the magnetic fields are flux frozen.

In this study we primarily focus on the subsequent evolution of this initially flux frozen magnetic fields in the viscous drag regime. As discussed in the main text, the evolution of magnetic field power spectrum is determined by eq. (4). Here, we shall focus on maximally helical magnetic fields,  $h(k) = 1$ . In this limit, the solution to eq. (4) is given by

$$P_B(k, k_D(t)) = P_B(k, t_i) e^{b(k_D)k/k_D - k^2/k_D^2}, \quad (11)$$

where  $b$  represents the feedback from inverse cascade,  $k_D$  represents the damping scale due to photon drag, and  $P_B(k, t_i)$  is the power spectrum of the magnetic fields after silk damping suppresses MHD turbulence. We borrow the shape of  $P_B(k, t_i)$  from Ref. [32], which obtained the power spectra after numerically simulating turbulent MHD evolution of magnetic fields. On scales larger than coherence length scales,  $P_B(k, t_i) \propto k^2$ , while on smaller scales,  $P \propto k^{-11/3}$ , according to Kolmogorov cascade.

The parameter  $b$  above can be expressed just as a function of  $k_D$ . To find this dependence, we substitute the above

equation back in eq. (4), to obtain

$$\frac{\partial b}{\partial \ln k_D} = -\frac{\int d\Pi_q (2q - b)P_B(q, k_D)}{k_D \int d\Pi_q P_B(q, k_D)}, \quad (12)$$

where  $d\Pi_q = d^3q/(2\pi)^3$ . In the left panel of figure 4, we show how  $b$  depends on  $k_D$  after numerically solving the above equation and setting  $b(t_i) = k_D^{-1}(t_i) = 0$ . This choice of initial condition is irrelevant as we find  $b$  to asymptote to the same values as long as we impose  $b(t_i) \ll 1$  and  $k_D^{-1}(t_i) \ll \xi_I$ . Here  $\xi_I$  is the coherence length scale of  $P_B(k, t_i)$ .

The expression for  $b$  is simplified in the limit  $k_D \ll \xi_I$ , where we can approximate  $P \propto k^{n_B} e^{bk/k_D - k^2/k_D^2}$  and  $b \gg 1$ . With this simplification we obtain

$$b = 2\sqrt{(2 + n_B) \ln(c/k_D)}. \quad (13)$$

For the  $P_B(k, t_i)$  used here (with  $n_B = 2$ ), we numerically find  $c \approx 0.3\xi_I^{-1}$  to accurately track evolution of  $b$  for  $k_D < \xi_I/10$ , as seen in the left panel of figure 4. Substituting the evolution of  $b$  in the evolution of  $k_D$ , in eq. (7), one obtains that  $k_D^{-1} \propto a(\ln a)^{(n_B+2)/6}$  and  $\langle B^2 \rangle \propto a^{-1}(\ln a)^{(n_B+2)/2}$ , which is in agreement with the simulations where the observed evolution is  $k_D \propto B^2 \propto a^{-1}$  [28].

As  $b$  evolves slowly with  $k_D$ , the exponential feedback from inverse cascade is limited to scales near  $k_D$ . In the right panel of figure 4, we show the evolution of  $E = k^2 P_B(k)$  at different  $k_D$  values. As  $k_D^{-1}$  becomes larger than  $\xi_I$ , the inverse helical cascade causes power to shift to larger scales such that the peak of  $E(k)$  remains largely unchanged.

### Magnetic damping scale for incompressible fluid

In this section we derive the evolution of non-helical magnetic field power spectrum for scenarios where the baryon thermal pressure dominates over the Lorentz force in the photon drag regime.

In the main letter we showed that the baryon velocity is determined by the balance between the Lorentz force and the photon drag force,  $a\vec{v}_b \approx \vec{L}_B/(\alpha + H)$ , when thermal pressure is negligible. In contrast, in the strong thermal pressure limit, compressible motion in the baryons is suppressed,  $\nabla \cdot v_b \rightarrow 0$ . However, the Lorentz force can induce divergence free motion in the baryon fluid without hindrance. Consequently, one can write the Fourier transformed baryon velocity vector as

$$v_{b,j}(q) = \left( \delta_{lj} - \frac{q_l q_j}{q^2} \right) \frac{L_{B,l}(q)}{a(\alpha + H)} = \hat{p}_{lj}(q) \frac{L_{B,l}(q)}{a(\alpha + H)}, \quad (14)$$

where  $\vec{L}_B(q)$  is the Fourier transform of the Lorentz force,  $\vec{L}_B(x) = (\nabla \times \vec{B}) \times \vec{B}/[4\pi a^4 \rho_b]$ .

The motion in the baryon fluid feeds back onto the magnetic field via the induction equation, eq. (2). Taking the Fourier transform of eq. (2) and replacing  $v_b$  using eq. (14), we obtain

$$\frac{\partial B_i(k)}{\partial t} = \frac{-k_m}{(4\pi\rho_b)(\alpha + H)} [\delta_{ml}\delta_{ji} - \delta_{mj}\delta_{li}] [\delta_{ab}\delta_{nc} - \delta_{bc}\delta_{na}] \int d\Pi_{q_1} d\Pi_{q_2} \hat{p}_{jn}(q_1) q_{2a} B_b(q_1 - q_2) B_c(q_2) B_l(k - q_1), \quad (15)$$

where  $d\Pi_q = d^3q/(2\pi)^3$ .

To obtain the evolution of the power spectrum, we use the fact that

$$\delta^3(k - k') \frac{\partial P_B(k)}{\partial t} = \frac{1}{2} \left\langle \frac{\partial B_m(k)}{\partial t} B_m^*(k') \right\rangle. \quad (16)$$

Then replacing the derivative of  $B$  using eq. (15), using  $\langle B_i(k) B_j^*(k') \rangle \equiv \delta^3(k - k') M_{ij}(k')$ , and assuming magnetic fields to be Gaussian distributed, we obtain

$$\begin{aligned} \frac{\partial P_B(k)}{\partial t} &= \frac{-\delta^3(k - k')}{2(4\pi\rho_b)(\alpha + H)} k_i [\delta_{il}\delta_{jm} - \delta_{ij}\delta_{lm}] [\delta_{ab}\delta_{nc} - \delta_{bc}\delta_{na}] \\ &\quad \times \int d\Pi_q \hat{p}_{jn}(k - q) [k_a M_{lb}(q) M_{cm}(k) - q_a M_{lc}(q) M_{bm}(k)]. \quad (17) \end{aligned}$$



Next, considering non-helical fields, we replace  $M$  using eq. (3) and set  $h = 0$ . Doing so yields

$$\frac{\partial P_B(k)}{\partial t} = \frac{-P_B(k)}{(4\pi\rho_b)(\alpha + H)} \int d\Pi_q \left[ -\frac{2}{3}(k^2 + 3q^2) + \frac{(k^4 + k^2q^2 + q^4)}{kq} \ln \left( \frac{k^2 + q^2 + kq}{k^2 + q^2 - kq} \right) \right] P_B(q). \quad (18)$$

To obtain a simple expression we can look at the asymptotic limit,  $k \ll k_D$  or  $k \gg k_D$ . In these limits, the integral is dominated by the phase space where  $q \sim k_D \gg k$  or  $q \sim k_D \ll k$ . Both limits yield

$$\frac{\partial P_B(k)}{\partial t} \approx -\frac{4k^2V_A^2}{3a^2(\alpha + H)} P(k), \quad (19)$$

where  $V_A^2 = \langle B^2 \rangle / [4\pi a^4 \rho_b]$  is the Alfvén speed.

Thus, we can see that the magnetic power spectrum evolution is well approximated by  $P(k, t) = P(k, t_i) e^{-k^2/k_D^2}$  for  $k$  values well separated from  $k_D$ . The evolution of the damping scale,  $k_D^{-1}$ , can be obtained by plugging this solution back in eq. (19). Doing so surprisingly yields the exact same equation as for compressible fluid, eq. (7).

While deriving the power spectrum evolution here and in the main letter, we considered that  $v_b \propto L_B$  on all scales. However, for  $k > k_D$ , the magnetic fields are being exponentially damped and for large enough  $k$ , the baryon flow should stop following the Lorentz force. However, as long as the scale where baryons stop following the Lorentz force is much smaller than  $k_D^{-1}$  we can safely assume  $v_b \propto L_B$  to always be valid for the purpose of evaluating  $P_B(k, t)$ . In particular, one can see that  $L_B$  is roughly suppressed as  $\sim k^2/k_D^2$  for  $k > k_D$  while  $v_b$  can at best decrease with a dimensionless rate of  $(H + \alpha)/H$ . Consequently,  $v_b$  follows the Lorentz force until  $k \gtrsim \sqrt{\alpha/H} k_D$ . Prior to recombination,  $\alpha$  is at least 300 times larger than  $H$ , so baryons follow the Lorentz force deep into the damping regime.

### Non-linear term in the baryon continuity equation

In this section we show that the non-linear term in the baryon continuity equation tends to enhance the baryon power spectrum when baryons are driven by magnetic fields.

We begin with the baryon continuity equation,

$$\frac{\partial \delta_b}{\partial t} + \frac{\nabla \cdot \vec{v}_b}{a} + \frac{\nabla \cdot (\vec{v}_b \delta_b)}{a} = 0. \quad (20)$$

Taking the Fourier transform of the above equation and then ensemble averaging with  $\delta_b^*(k')$ , we obtain

$$\left\langle \frac{\partial \delta_b(k)}{\partial t} \delta_b^*(k') \right\rangle + \frac{\langle \vec{k} \cdot \vec{v}_b(k) \delta_b^*(k') \rangle}{a} + \delta^3(k - k') \Xi(k) = 0, \quad (21)$$

where  $\delta^3(k) = (2\pi)^3 \delta(k)$  and

$$\delta^3(k - k') \Xi(k) \equiv -\frac{i}{a} \int \frac{d^3q}{(2\pi)^3} \langle (\vec{k} \cdot \vec{v}_b(q)) \delta_b(k - q) \delta_b^*(k') \rangle. \quad (22)$$

Here  $\Xi(k)$  represents the contribution from the non-linear term in eq. (20) to the evolution of the baryon density power spectrum.

We are primarily interested in the regime where baryon perturbations become non-linear, i.e. where the Lorentz force dominates over the baryon thermal pressure and gravity. Consequently,  $v_b$  is determined by the balance between the Lorentz force and the photon drag force,  $a\vec{v}_b \approx \vec{L}_B/(\alpha + H)$ . Furthermore, assuming that  $\delta_b$  is largely determined by the linear continuity equation, eq. (20), we have  $\delta_b = -C\nabla \cdot v_b/[aH] = -C\nabla \cdot \vec{L}_B/[a^2H(\alpha + H)]$ , where  $C$  is some constant of motion. As both  $v_b$  and  $\delta_b$  are now expressed in terms of the Lorentz force, we can simplify eq. (22) to obtain  $\Xi$  in terms of the magnetic field power spectrum,

$$\Xi(k) = \frac{-4C^2[\delta_{ml}k_j - \delta_{mj}k_l](k_r k_s - k^2 \delta_{rs}/2)}{(4\pi a^4 \rho_b)^3 a^6 (H + \alpha)^3 H^2} \int d\Pi_q d\Pi_{q_1} [(k - q - q_1)_u (k - q - q_1)_v - (k - q - q_1)^2 \delta_{uv}/2] \\ \times (q_1 - q)_m M_{jr}(q_1) M_{lu}(q) M_{vs}(k - q_1), \quad (23)$$

where  $M$  is defined through  $\langle B_i(k) B_j^*(k') \rangle \equiv \delta^3(k - k') M_{ij}(k')$  and  $d\Pi_q = d^3q/(2\pi)^3$ . While obtaining the above expression, we assumed the magnetic fields to be Gaussian distributed. In what follows, we shall show that  $\Xi$  is largely negative and hence leads to an enhancement of the baryon power spectrum.

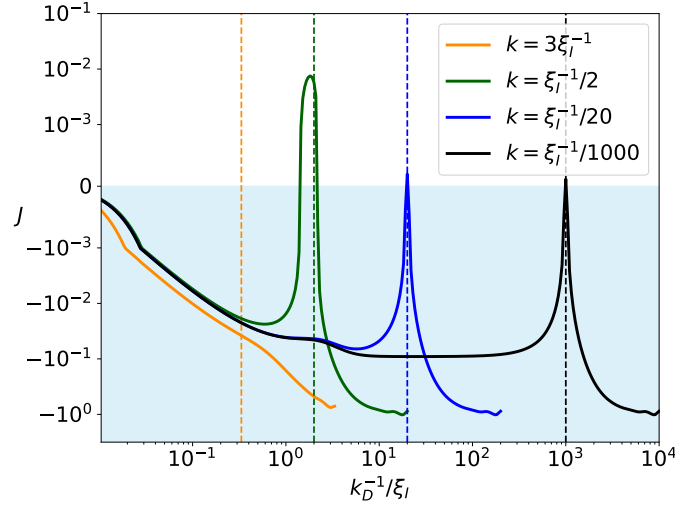


FIG. 5. Figure shows  $J$ , which parametrizes the impact of the non-linear term in the baryon continuity equation, as a function of the damping scale,  $k_D^{-1}$ , for different values of  $k$ . The vertical dashed lines mark the points where  $k_D = k$ . We can see that  $J$  is almost always negative, except for small region near  $k = k_D$ . The negative values of  $J$  imply that the non-linear term enhances the linear baryon power spectrum.

We can further simplify the above integral by considering maximally helical magnetic fields with  $M$  given by eq. (3) after setting  $h(k) = 0$ . Then after contracting over all indices and integrating over  $q$ , we obtain

$$\begin{aligned} \Xi(k) = & \frac{C^2}{(4\pi a^4 \rho_b)^2 a^6 (H + \alpha)^3 H^2} \frac{1}{8} \frac{2V_A^2}{3} k^3 \int d\Pi_{q_1} P_B(q_1) \frac{P_B(k - q_1)}{(\vec{k} - \vec{q}_1)^2} \\ & \left( k q_1 \left[ q_1^3 (1 - 3x^2 + 2x^4) - k q_1^2 x (1 - 5x^2 + 4x^4) + k^2 q_1 (1 - 5x^2 + 4x^4) + k^3 x (1 - x^2) \right] \right. \\ & \left. + k_{*n}^2 k_D^2 \left[ 2q_1^3 x^3 - 2k q_1^2 x^2 (x^2 + 2) + 3k^2 q_1 x (1 + x^2) - k^3 (1 + x^2) \right] \right). \end{aligned} \quad (24)$$

where  $x = (\vec{k} \cdot \vec{q}_1)/k q_1$ ,  $V_A^2 = \int d\Pi_q P_B(q)/[4\pi a^4 \rho_b]$ , and  $k_{*n}$  represents the moments of the magnetic power spectrum,

$$k_{*n}^n \equiv \frac{\int d\Pi_q q^n P_B(q)}{\int d\Pi_q P_B(q)}. \quad (25)$$

The integral in  $\Xi(k)$  is similar to the integral in the power spectrum of the Lorentz force [54],

$$\begin{aligned} \langle \nabla \cdot \vec{L}_B(k) \nabla \cdot \vec{L}_B(k') \rangle = & \delta^3(k - k') P_{\nabla \cdot \vec{L}_B} = \delta^3(k - k') \frac{k^4}{8(4\pi a^4 \rho_b)^2} \int \frac{d^3 q}{(2\pi)^3} \frac{P_B(q) P_B(k - q)}{(k - q)^2} \left[ k^2 (1 + x^2) - 4k q x^3 \right. \\ & \left. + 2q^2 (1 - 2x^2 + 2x^4) \right]. \end{aligned} \quad (26)$$

Consequently, we rewrite  $\Xi$  in terms of  $P_{\nabla \cdot \vec{L}_B}$  and use the fact that we have assumed  $\delta_b = -C \nabla \cdot \vec{L}_B/[a^2 H(\alpha + H)]$ , to obtain

$$\Xi(k) = \frac{C^2 P_{\nabla \cdot \vec{L}_B}}{a^6 (H + \alpha)^3 H^2} \frac{2k_D^2 V_A^2}{3} J(k, k_D) = \frac{2P_b(k)}{3} \frac{k_D^2 V_A^2}{a^2 (H + \alpha)} J(k, k_D), \quad (27)$$

where  $\delta^3(k - k') P_b(k) = \langle \delta_b(k) \delta_b^*(k') \rangle$ , and  $J$  is a dimensionless quantity that parametrizes the ratio of the integrals in  $\Xi$  and  $P_{\nabla \cdot \vec{L}_B}$ .

Since  $\Xi$  is proportional to  $P_b$ , we can effectively rewrite the continuity equation for baryon as

$$\frac{\partial \delta_b}{\partial t} + \frac{\nabla \cdot \vec{L}_B}{a(\alpha + H)} + \frac{2\delta_b}{3} \frac{k_D^2 V_A^2}{a^2 (H + \alpha)} J(k, k_D) = 0, \quad (28)$$

where we have used  $a\vec{v}_b \approx \vec{L}_B/(\alpha + H)$ . The above equation would yield the same equation for  $P_b$  as the original continuity equation when baryons are driven by the Lorentz force.

The above equation also allows us to confirm our original assumption of  $\delta_b = -C\nabla \cdot \vec{L}_B/[a^2H(\alpha + H)]$ . To do so we simply substitute  $\delta_b = -C\nabla \cdot \vec{L}_B/[a^2H(\alpha + H)] \propto a^m$  in eq. (28) to obtain,

$$C = \frac{1}{m + \left[ \frac{2}{3} \frac{k_D^2 V_A^2}{a^2(H+\alpha)} J(k, k_D) \right]}. \quad (29)$$

Note that  $\frac{k_D^2 V_A^2}{a^2(H+\alpha)} \sim \mathcal{O}(1)$  according to the definition of  $k_D$  (eq. (7)). Consequently, the non-linear term in the continuity equation simply provides a correction of order  $J/m$  to the linear solution. In a radiation-dominated universe, we have  $m = 3$  prior to the damping of the magnetic fields.

In figure 5, we show  $J$  as a function of  $k_D$  for different values of  $k$ . Note that  $J$  is typically of order  $-0.1$  for  $k < k_D$ . For  $k \sim k_D$  we see  $J$  to jump to a small positive value and then it again becomes negative. The large negative values of  $J$  for  $k \gg k_D$  have no physical significance because in that limit the magnetic fields and  $v_b$  are exponentially damped. Consequently, our calculation of  $\Xi$ , which is based on the assumption of  $\delta_b \propto \vec{v}_b/a$ , is no longer applicable. We instead expect  $\Xi$  to go to zero for  $k \gg k_D$  because  $\delta_b$  is no longer correlated with  $\vec{v}_b \approx \vec{L}_B/(\alpha + H)$ .

Hence, when the growth in  $\delta_b$  is sourced by the magnetic fields, we expect the non-linear terms in the baryon continuity equation to provide a small enhancement to the baryon power spectrum obtained from linear analysis.